Electrochemical and Solid-State Letters, **13** (9) K77-K79 (2010)
1099-0062/2010/13(9)/K77/3/$28.00 © The Electrochemical Society

Structure and Interfacial Properties of Germanium Nanowires Grown on Titanium

Brian A. Bryce,[a,z] Mark P. Levendorf,[b] Jiwoong Park,[b] and Sandip Tiwari[c]

[a]*School of Applied and Engineering Physics,* [b]*Department of Chemistry and Chemical Biology, and* [c]*School of Electrical and Computer Engineering, Cornell University, Ithaca, New York 14853, USA*

Single-crystal germanium nanowires have been grown directly on amorphous titanium films using the vapor–liquid–solid method and studied using transmission electron microscopy. Forty nanometer wires are observed to grow only in the ⟨111⟩ and ⟨112⟩ directions and have a sharp (~1 nm) metal–semiconductor interface to both the catalyst (Au) and the titanium substrate. They exhibit a defective base region comparable in size to the catalyst diameter terminated by a kink structure after which they are single crystalline. The physical characteristics of these nanowires are examined. A simple lithographic method to produce grids for rapid characterization is introduced.
© 2010 The Electrochemical Society. [DOI: 10.1149/1.3457852] All rights reserved.

Manuscript submitted April 14, 2010; revised manuscript received May 25, 2010. Published July 1, 2010.

Nanowires have been explored in electronics[1-3] to achieve desirable device properties and recently for photovoltaics as an alternative to planar single-crystal structures.[4-7] The latter is particularly attractive. Silicon and germanium wires can have a distribution in properties, size, bulk and surface defects, lifetime, etc., and yet allow the formation of coaxial diode structures useful in energy conversion while being produced using potentially low cost growth techniques such as vapor–liquid–solid (VLS) growth.[8] The cells produced to date using bottom-up methods such as VLS have generally had conversion efficiencies $<1\%$.[4-6] Individual devices have measured efficiencies as high as 3.4%.[7] Causes for these low efficiencies include material recombination losses, transport characteristics, and device parasitics arising from the contact interfaces.

Previous studies have shown that semiconductor wire cells achieve a performance improvement over planar cells in a limited window of wire size and crystal quality.[9] This constrains the application of VLS wires to lower cost, lower efficiency designs than the best planar cells. Single-crystal substrates allow wires to be grown epitaxially[10] and many attempts to produce wire solar cells have relied on such substrates to achieve the highest possible material quality. Although this approach is useful in systematically isolating wire quality as the limiting factor in cell design, such cells are not practical because the growth substrate adds significantly to cell cost. If a matched single-crystal semiconductor wafer could be replaced with an inexpensive metal film while maintaining wire quality, density, and a low contact resistance to the wires, the overall cost of a VLS wire solar cell would be greatly reduced.

Group IV VLS wires grown directly on metal films have been reported.[6] Although this report expressed concerns of possible metal film/wire interactions, they did not examine the structures or interfaces directly. Such an examination is important. Minority carrier devices depend critically on material quality. The metal/wire interfacial properties directly impact parasitic contact effects and transport in any device structures.

In this article, we explore the possibility of using Ti as a replacement for single-crystal wafers in conjunction with Au catalyzed VLS Ge nanowires by directly observing the material properties of the resulting nanostructures with particular emphasis on the substrate interface and early wire growth. Ti was selected for its stable insulating oxide, abundance, cost, and formation of ohmic contacts to both Ge and Si. Ge was selected for its large optical absorption coefficient and low growth temperature relative to Si.

Long, straight, high quality Ge nanowires can be grown on bulk grade 2 Ti sheets as well as Ti thin films (Fig. 1a). For this work, short nanowires grown on thin films were principally used; thin films of Ti on Si simplify clean room processing; short wires contain all interfaces and regions of interest and are less sensitive to vibrations during observation.

Synthesis of the Ge nanowires was carried out in a 1 in. quartz tube furnace in an atmosphere of GeH_4:H_2. The total pressure was 100 Torr and the GeH_4 partial pressure was 1.5 Torr. Colloidal Au particles with diameters ~40 and ~80 nm were used as the growth catalyst. The colloids were deposited on the Ti film after treatment with poly-L-lysine (0.1% w/v). Optimum growth for Ge wires occurred in the 310–330°C range. Although these temperatures are below the bulk eutectic point of the Ge–Au system, VLS can occur in Ge wires below the bulk eutectic point.[11]

Grids for transmission electron microscopy (TEM) were prepared both by the commonly used mechanical removal of the nanowires onto a carbon-coated grid and by a lithographic method that is described here. For carbon grid samples, nanowires were grown under the conditions outlined above on a 250 nm Ti film and were observed via scanning electron microscopy (SEM) before their mechanical removal onto the grid.

Lithographic samples were produced from ⟨111⟩ Si wafers. A thin electron transparent (minor) ridge ≈100 nm × 1 μm was defined via reactive ion etching (RIE) perpendicular to the ⟨110⟩ direction. A second 40 × 40 μm (major) ridge was then defined via RIE with the first ridge in the center (Fig. 1b). After defining the second ridge, the wafer was diced parallel to each ridge into thin 250 μm wide strips with each strip containing one double ridge structure. Following this dicing step, a thin film of Ti (25 nm) was evaporated and nanowire synthesis carried out as normal.

The use of a second (major) ridge allows for greater usable tilt about the axis parallel to the ridge structure. In this configuration, tilt about the axis parallel to the ridge structure is limited to the grazing angle (2.8°) of the ridge structure, whereas tilt in the perpendicular axis is limited by the microscope itself. The alignment of the double ridge perpendicular to the ⟨110⟩ direction allows for observation of epitaxy in samples grown directly on Si as well as calibration of the microscope.

This preparation method has several advantages that greatly increase throughput and yield over more commonly used methods. The nanowires are completely undamaged because all thinning occurs before synthesis. Observation of nanowires grown on top of the minor ridge is possible from tip to base even for wires that do not grow vertically so long as the wires are grown to a height less than the minor ridge (1 μm). The time to prepare a grid is short: After the lithographic patterning and nanowire growth is complete, it is limited to a simple cleave-and-glue step. The overhead to prepare many samples is low because a single 100 mm wafer can make as many as 4000 grids. The viewable area is large: The electron transparent ridge is several millimeters in length, which is 100 times longer than the transparent (<200 nm thick) length (≈10 μm) in a 1° wedge polished sample. The nanowires are not encapsulated in

[z] E-mail: bab79@cornell.edu

Downloaded 18 Jul 2010 to 128.84.158.108. Redistribution subject to ECS license or copyright; see http://www.ecsdl.org/terms_use.jsp

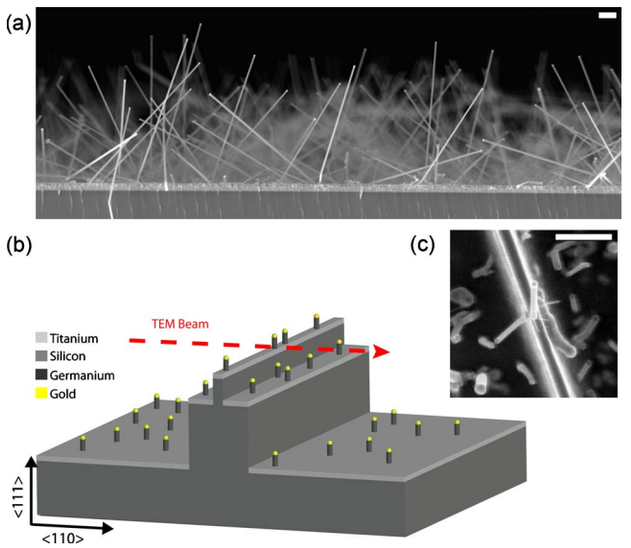

Figure 1. (Color online) (a) SEM of typical growth showing 40 nm Ge wires on a 250 nm Ti thin film (scale bar 500 nm). (b) Schematic showing the double ridge structure (not to scale). The minor ridge is ≈100 nm × 1 μm, the major ridge is 40 × 40 μm, and the supporting wafer is 250 μm wide. The structure is made from a ⟨111⟩ Si wafer and the ridge is oriented so that the ⟨110⟩ direction is perpendicular to the ridge. (c) Plan-view SEM of lithographic minor ridge after Ti evaporation and nanowire growth showing a single nanowire at the center of the ridge (scale bar 500 nm).

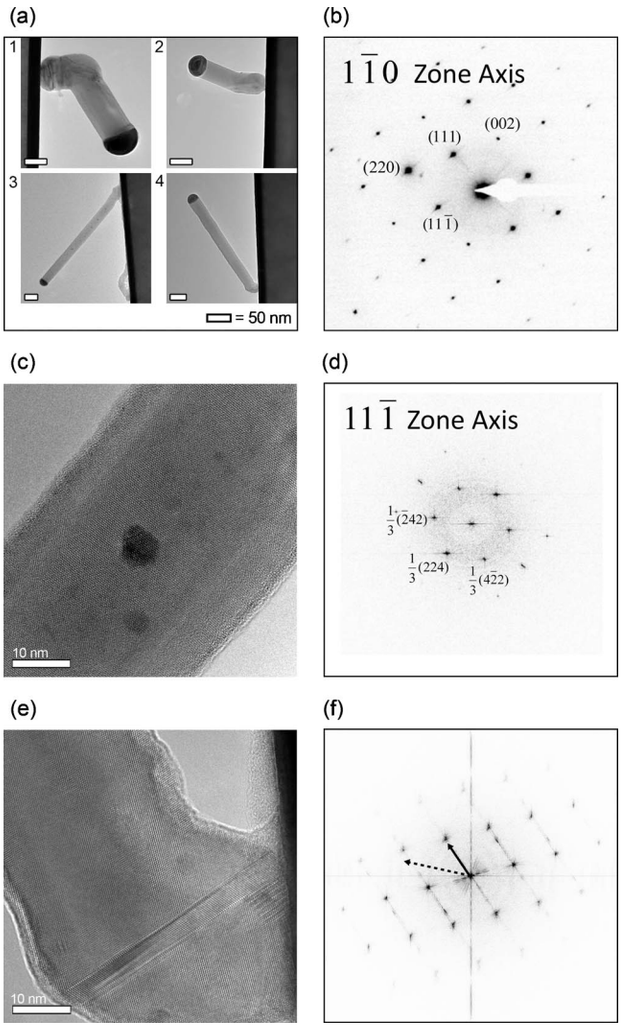

Figure 2. (a) Four examples of nanowires with kinks at the boundary between defective and defect-free regions; (b) selected area diffraction indexing of the nanowire in (a4) and (e) showing ⟨111⟩ growth direction; (c) HM-TEM showing sidewall bumps (dark areas), two side facets (edges), and low defect central area; (d) fast Fourier transform (FFT) indexing of wire in (c) showing ⟨112⟩ growth direction; (e) HM-TEM showing the base of wire in (a4) exhibiting defects and change in growth direction; and (f) FFT of (e). The dashed arrow indicates the initial growth direction as seen in (e), which is not in any low order direction; the solid arrow indicates the final growth in the ⟨111⟩ direction.

epoxy. This allows further SEM observation after the sample is produced and removes background carbon signals from compositional analysis.

Wires grown from ~40 and ~80 nm colloids were observed to have identical qualitative features in SEM. Lithographic grids offer the ability to observe the Ti–Ge interface and are mechanically more stable than carbon grids. Forty nanometer wires offer better electron transmission than 80 nm wires. Thus, the majority of our observations were made using lithographically prepared grids and ~40 nm wires.

Our principal use for carbon grid samples was in refining our lithographic grid process. For instance, we initially did not use a second (major) ridge in the lithographic process. Because the TEM beam is not perfectly collimated over 250 μm, we observed many artifacts. We were able to identify this problem by comparing the lithographic samples to carbon grid samples. In general, the fragments of wires available on carbon grid samples are qualitatively indistinguishable from the upper sections of the lithographic samples. This fact and the electron energy loss spectroscopy (EELS) data presented later suggest that the 25 nm Ti film on the lithographic samples may be treated as bulk.

High magnification transmission electron microscopy (HM-TEM) observations of 40 nm Ge wires show several interesting features. The nanowires do not grow in any preferred direction relative to the substrate, which is reasonable given the amorphous nature of the metal film. All observed 40 nm wires are strongly faceted single crystals growing in either the ⟨111⟩ or ⟨112⟩ direction (Fig. 2b and d). The observed fractional 1/3 {224} reflections[12] have been previously seen in similarly sized Si nanowires.[13] The nanowire side facets are flat with only a small amount of uncatalyzed chemical vapor deposition growth occurring in the form of small hemispherical bumps on the sidewall surfaces. These appear as contrast dots in HM-TEM (Fig. 2c) due to their lattice orientation mismatch with the underlying wire and are more readily identified as bumps via scanning transmission electron microscopy (STEM) (Fig. 3a). The wires do not exhibit the initial diameter taper of epitaxially grown wires.[14]

This implies that the Au–Ge eutectic has a contact angle greater than 90° to the growth surface. This growth surface is at least initially a thin amorphous TiO_2 layer created by the exposure of the Ti film to air. Pure Au has a nominal contact angle of 122° to TiO_2(110);[15] thus, the observed lack of wetting is not entirely surprising.

Nearly all nanowires observed consist of two parts: an upper nearly defect-free region and a defective region near the Ti thin film that is comparable in size to the catalyst diameter. This defective region consists of one or more grains that merge into a single-crystal wire. The transition between the defective region and the low defect region is marked by a change in the growth direction of the nanowire or "kink" (Fig. 2a). Although the wire changes growth directions, the crystal orientation relative to the substrate does not change at the kink. A variety of mechanisms can cause nanowires to kink.[16,17] In the wires under observation, kinking is needed to allow the nanowire to grow in the energetically favorable[18] ⟨111⟩ and ⟨112⟩ directions (Fig. 2e and f). These directions have the lowest

Downloaded 18 Jul 2010 to 128.84.158.108. Redistribution subject to ECS license or copyright; see http://www.ecsdl.org/terms_use.jsp

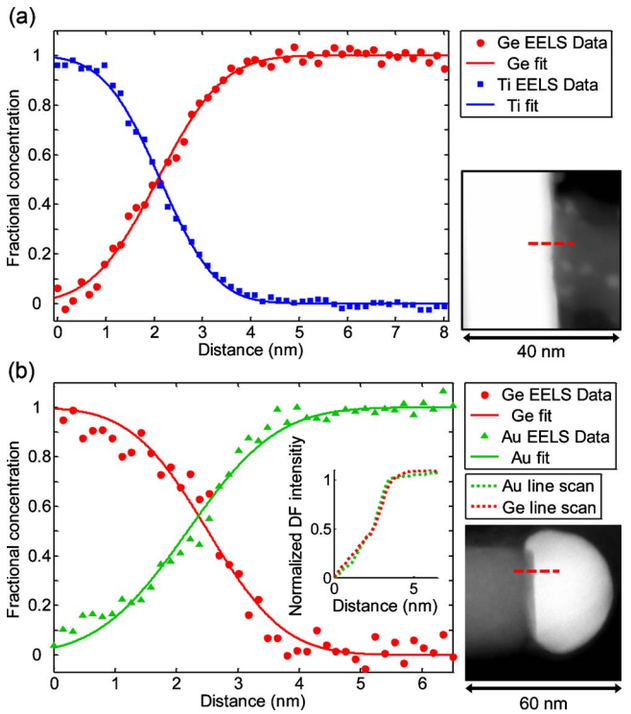

Figure 3. (Color online) EELS line scans of top and bottom wire/metal interfaces with data fitted to complementary error functions; the dashed lines in the STEM images shown at the right indicate the position of the line scans. (a) Ti/Ge interface (spectrometer dispersion 0.5 eV/channel) and (b) Au/Ge interface (spectrometer dispersion 0.3 eV/channel). The Au/Ge interface data were collected with two line scans due to the large energy separation of the EELS edges. The inset (b) dark field intensity shows the alignment of the two scans compensated for drift. The composition does not cross at 0.5 due to imperfect drift correction.

surface energy in a diamond lattice.[19] Although surface tension and other terms change the energy balance of the liquid–solid interface, at the size of the wires under study the surface energy term dominates and so two aforementioned directions are preferred. The reason why the ⟨111⟩ and ⟨112⟩ surfaces have the lowest energy follows intuitively from the surface energy being directly proportional to the number of dangling bonds on a surface.[20]

These observations suggest that at the Ti surface, there is no preferred direction for nucleation, so a randomly oriented crystal initially precipitates. As the growth of the crystal continues, the catalyst moves to the nearest energetically favorable facet. This movement, combined with the continual growth of the crystal, forms the kink. Once the catalyst reaches the energetically favorable facet, the wire growth proceeds as it would on a matched wafer: as a low defect single crystal. Some nanowires also contain kinks far away from the base region. These kinks do not serve as boundaries between defective and defect-free regions of the wire and are likely caused by another mechanism, such as motion in the position of the catalyst meniscus caused by a variation in the process parameters that disturbed the delicate balance of surface tension[18] at the wire tip.

The nanowires are not tapered. Given the lack of sidewall growth, this implies that there is no major Au migration or incorporation in the nanowires. EELS measurements of both the central wire and sidewall bumps show no detectable Ti or Au signals, implying that the bumps are uncatalyzed growths, which may simply nucleate on point defects in the crystal's sidewall.

EELS line scans of both the top and bottom metal/wire interfaces were also performed. The EELS data are consistent with a Gaussian beam with a standard deviation of ~1 nm sweeping over an atomically sharp interface and places an upper bound on the transition width (10–90%) of the Ti–Ge and Ge–Au interfaces of 2.4 and 2.9 nm, respectively (Fig. 3). The Ti film is an order of magnitude thicker than this upper bound, implying that the thin film can be treated as identical to the bulk. This minimal alloying is consistent with our expectations,[21] given our relatively low temperature (310–330°C) and short growth time (<10 min). This weak interaction is an important feature. If the rate of germanide formation had exceeded the wire growth rate, the resulting structure would simply have been a germanide of little use. Because the reverse is true, a two-step process is possible: First, grow the wires, and second, form the germanide needed for a low contact resistance.

Energy-dispersive X-ray measurements of the lithographically prepared samples show no detectable elemental contamination from processing. SEM observations show that the same morphologies are present on all sample types. Ge nanowires grown on Ti films are of comparable structural quality to Si control samples grown simultaneously. These control samples do not exhibit epitaxy due to the low temperatures used.

In summary, it is possible to grow high quality VLS Ge nanowires on Ti. These wires alloy minimally with the Ti surface because of the low growth temperatures used. The wires do contain a defective base region and have no preferred alignment due to the amorphous nature of the metal film. However, these are not major drawbacks in applications that do not require epitaxy. After device formation, it should be possible to form a low resistance contact at the Ti–Ge interface with a simple high temperature anneal. These characteristics show that Ti holds promise in replacing semiconductor wafers in VLS wire solar cells.

Acknowledgments

We thank the Muller group at Cornell and in particular Huolin Xin and John Grazul for their kind advice and help. This work was supported by the Cornell Center for a Sustainable Future (CCSF), the NSF IGERT Program, the Cornell Center for Materials Research (CCMR), and partly performed at the Cornell Nanoscale Facility.

The Cornell Center for a Sustainable Future assisted in meeting the publication costs of this article.

References

1. C. K. Chan, H. Peng, G. Liu, K. McIlwrath, X. F. Zhang, R. A. Huggins, and Y. Cui, *Nat. Nanotechnol.*, **3**, 31 (2008).
2. J. Xiang, W. Lu, Y. Hu, Y. Wu, H. Yan, and C. M. Lieber, *Nature (London)*, **441**, 489 (2006).
3. F. Qian, S. Gradečak, Y. Li, C. Wen, and C. M. Lieber, *Nano Lett.*, **5**, 2287 (2005).
4. T. Stelzner, M. Pietsch, G. Andrä, F. Falk, E. Ose, and S. Christiansen, *Nanotechnology*, **19**, 295203 (2008).
5. O. Gunawan and S. Guha, *Sol. Energy Mater. Sol. Cells*, **93**, 1388 (2009).
6. L. Tsakalakos, J. Balch, J. Fronheiser, B. A. Korevaar, O. Sulima, and J. Rand, *Appl. Phys. Lett.*, **91**, 233117 (2007).
7. B. Tian, X. Zheng, T. J. Kempa, Y. Fang, N. Yu, G. Yu, J. Huang, and C. M. Lieber, *Nature (London)*, **449**, 885 (2007).
8. R. S. Wagner and W. C. Ellis, *Trans. Metall. Soc. AIME*, **233**, 1053 (1965).
9. B. M. Kayes, H. A. Atwater, and N. S. Lewis, *J. Appl. Phys.*, **97**, 114302 (2005).
10. H. Adhikari, A. F. Marshall, C. E. D. Chidsey, and P. C. McIntyre, *Nano Lett.*, **6**, 318 (2006).
11. S. Kodambaka, J. Tersoff, M. C. Reuter, and F. M. Ross, *Science*, **316**, 729 (2007).
12. J. M. Gibson, M. Y. Lanzerotti, and V. Elser, *Appl. Phys. Lett.*, **55**, 1394 (1989).
13. Y. Wu, Y. Cui, L. Huynh, C. J. Barrelet, D. C. Bell, and C. M. Lieber, *Nano Lett.*, **4**, 433 (2004).
14. V. Schmidt, S. Senz, and U. Gösele, *Appl. Phys. A: Mater. Sci. Process.*, **80**, 445 (2005).
15. L. Zhang, F. Cosandey, R. Persaud, and T. E. Madey, *Surf. Sci.*, **439**, 73 (1999).
16. T. Kawashima, T. Mizutani, H. Masuda, T. Saitoh, and M. Fujii, *J. Phys. Chem. C*, **112**, 17121 (2008).
17. Y. Hyun, A. Lugstein, M. Steinmair, E. Bertagnolli, and P. Pongratz, *Nanotechnology*, **20**, 125606 (2009).
18. V. Schmidt, S. Senz, and U. Gösele, *Nano Lett.*, **5**, 931 (2005).
19. J.-M. Zhang, F. Ma, K.-W. Xu, and X.-T. Xin, *Surf. Interface Anal.*, **35**, 805 (2003).
20. S. B. Zhang and S.-H. Wei, *Phys. Rev. Lett.*, **92**, 086102 (2004).
21. O. Thomas, S. Deiage, F. M. d'Heurle, and G. Scilla, *Appl. Phys. Lett.*, **54**, 228 (1989).

Downloaded 18 Jul 2010 to 128.84.158.108. Redistribution subject to ECS license or copyright; see http://www.ecsdl.org/terms_use.jsp